Supporting Information for:

Enhanced Plasmonic Trapping and Fluorescent Emission of Nitrogen-Vacancy Nanodiamonds Using a High-Efficiency Nanofocusing Device

Boqun Liang[1], Yaodong Xu[1], Ning Yu[2], Zhaoxi Yang[2], Matthew Wilson[3], Da Xu[4], Rifat Ara Shams[4], Longjian Wang[4], Chun Hung (Joshua) Lui[3], Ruoxue Yan[2,4], Ming Liu[1,4*]

Addresses:

[1] *Materials Science and Engineering program, University of California – Riverside, Riverside, California 92521, United States*

[2] *Department of Chemical and Environmental Engineering, University of California – Riverside, Riverside, California 92521, United States*

[3] *Department of Physics and Astronomy, University of California – Riverside, Riverside, California 92521, United States*

[4] *Department of Electrical and Computer Engineering, University of California – Riverside, Riverside, California 92521, United States*

KEYWORDS:

Fluorescent Nano-diamond, plasmonic optical trapping, plasmonic coupling, silver nanowire

Email: mingliu@ucr.edu

Contents

1. Optical setup for PL imaging

For PL excitation, a 532-nm continuous wave laser (Laser Quantum Ventus) is channeled through a single-mode optical fiber to the OF-AgNW probe. The tip of the OF-AgNW probe is positioned within a polydimethylsiloxane (PDMS) fluidic channel. The FND solution (Adámas carboxylated red FNDs), diluted to 1/10,000th of its original concentration, is introduced into one port of the PDMS channel, allowing it to diffuse towards the plasmonic trap. FNDs undergoing Brownian motion are captured by the plasmonic potential at the AgNW tip. For fluorescence observation, an optical microscope (Nikon, Eclipse Ni-U, LU plan Fluor 50× objective lens, NA = 0.5) paired with an s-CMOS) camera (Andor, Zyla 5.5) is utilized. A long-pass filter (FEL 550, Thorlabs) and a notch filter (NF533-17, Thorlabs) are employed to obstruct the 532 nm excitation laser. Video recording is conducted at an exposure time of 35 ms per frame.

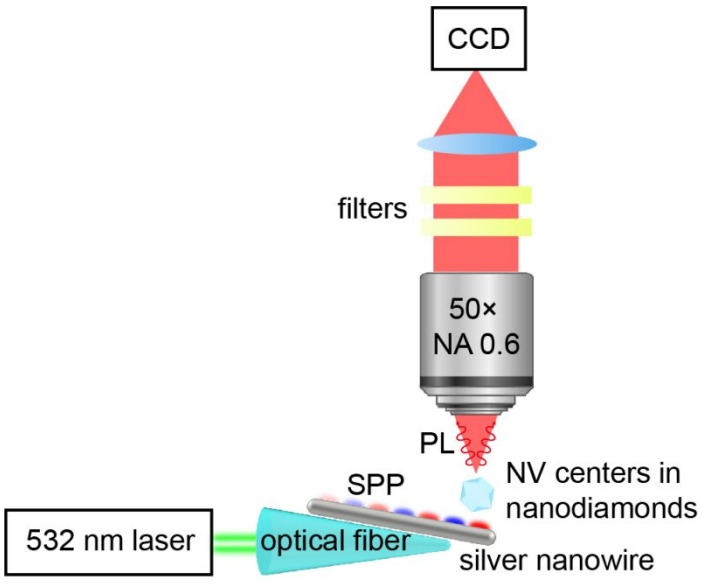

Figure S1. The schematic of the optical setup for particle dynamics analysis.

2. Long-Term Dynamics and Efficiency of Plasmonic Trapping with Multiple FNDs

We have also demonstrated the capability of the plasmonic trapping probe to maintain the capture of multiple FNDs over extended operational periods. As illustrated in Figure S2, after approximately 5 minutes of continuous operation, several FNDs have accumulated at site A, producing an average count rate of approximately 20,000 cps as shown in Figure S2c. The dynamic interaction of FNDs approaching site A results in observable 'sparkles' at both site A and site B, with site B serving as a scatterer affixed to the AgNW. This site consistently displays a lower average intensity, around 1,000 cps.

The assembly of multiple FNDs at site A impacts the trapping dynamics significantly. The accumulated FNDs effectively reduce the available plasmonic force at the tip of the AgNW, hindering the attachment of new FNDs. Consequently, isolated trapping events are observed in Figure S2c and d. Moreover, these previously trapped FNDs at site A begin to function as scatterers themselves, enhancing local scattering into free space. This scattering notably diminishes the coupling efficiency of incoming FNDs to the SPP on AgNW. This effect is quantitatively confirmed in the intensity correlation shown in Figure S2e, where the intensity ratio between site B and site A drops to 0.32, a marked decrease from the ratio of 5.3 observed with pristine AgNWs, indicating that must less light is coupled to the SPP channel. Interestingly, a branch of correlation with a higher ratio, approximately 1.0, indicates the presence of another FND (FND 2) positioned near site B, as captured in Frame #667 (Figure S2b).

Furthermore, the cross-correlation analysis depicted in Figure S2f reinforces the high degree of correlation between sites A and B, confirming that the emissions from these sites originate from the same quantum emitter. This analysis underscores the complex interplay of forces and interactions at work in long-term plasmonic trapping scenarios, revealing both the limitations and dynamic processes governing the system. The observed decrease in coupling efficiency due to

FND accumulation provides critical insights into the scalability and operational thresholds of plasmonic trapping systems, guiding future improvements in probe design and functionality.

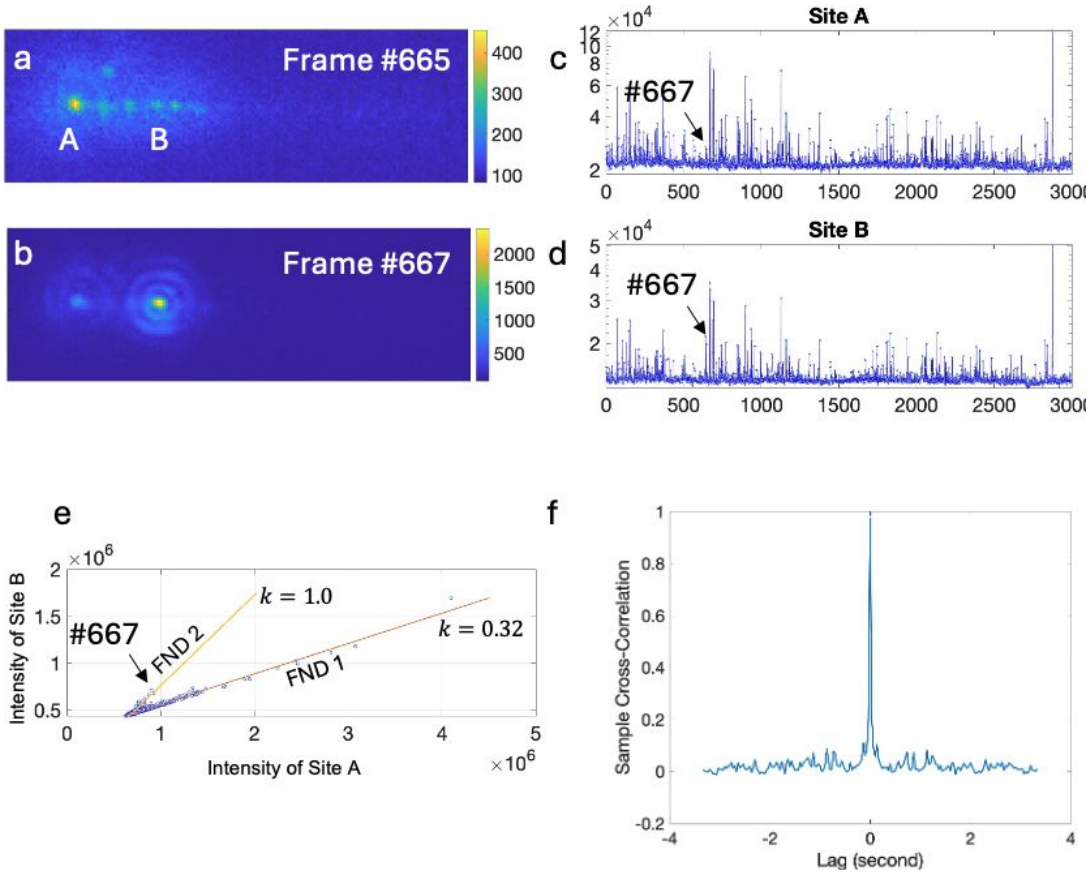

Figure S2. **Analysis of Plasmonic Trapping and Fluorescence on a Nanowire.** (a) Image of luminescent spots at sites A and B during long-time trapping (Frame #665). (b) At Frame #667, a second FND particle approaches Site B. (c) and (d) Time-resolved fluorescence intensity at sites A and B, respectively, with a notable peak at Frame #667 primarily at Site B. (e) Intensity correlation between sites A and B, indicating different FND contributions with correlation slope $k = 0.32$ for an FND at Site A and $k = 1$ for an FND at Site B. (f) Sample cross-correlation, confirming synchronous fluorescence signals from the same quantum emitter.

3. Simulations for Purcell factor distribution

Finite element analysis is employed for the numerical simulations reported in this study. For computing the Purcell factor, an electric dipole is positioned at various locations near a silver nanowire (100 nm in radius) to assess radiation power. The surrounding dielectric, encompassing both the dipole and AgNW, is assigned a permittivity of 1.76, replicating the conditions of water. In the experimental setup, the excitation laser is introduced through an optical fiber to stimulate the SPP on the AgNW waveguide. Correspondingly, in the simulation, the SPP in HE_1 mode profile is initiated from the end of the AgNW that connected to the simulation boundary (the red port in Figure S3a). Perfectly matched layers (PML) are applied to absorb the scattered light and reflected SPP. The resulting electric field distribution from this process is then applied to define the electric dipole's magnitude in the following simulations for the radiation power enhancement. As illustrated in Figure S3a, the total power emitted by the dipole is determined by integrating the time-averaged Poynting vectors over a virtual spherical boundary (blue sphere) that encases the dipole[1-3]. To establish a baseline for normalization, the radiation power from a standalone electric emitter I_0 is calculated, assuming an excitation by the same laser power under diffraction limit

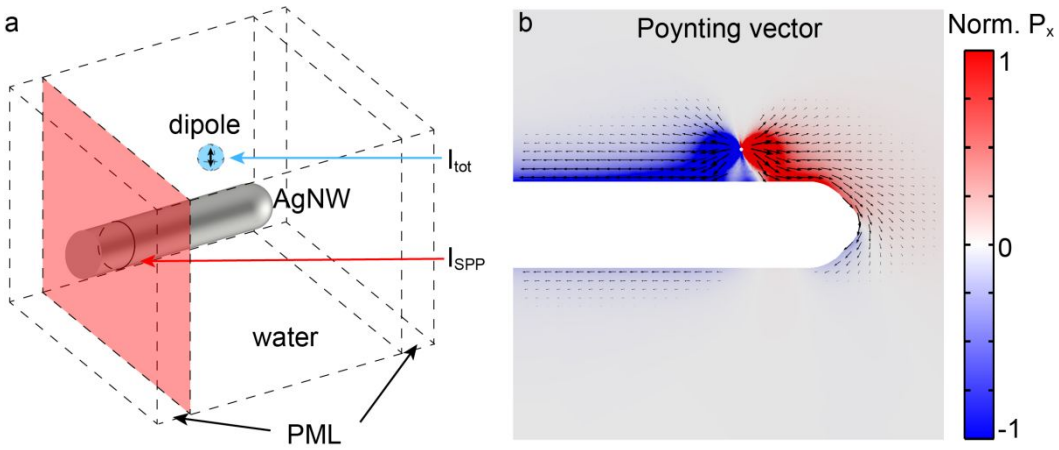

Figure S3. Simulations for dissipation channel analysis. (a) Simulation domains and power calculations. (blue: boundaries used for I_{tot} , red: boundaries used for I_{SPP}). (b) Poynting vector (arrow) and its *x*-direction component magnitude (color map) mapping the energy flux from a dipole emitter placed next to the AgNW.

focus. The Purcell factor (F_{P}) is subsequently defined as $F_{\mathrm{p}} = \frac{I_{\mathrm{tot}}}{I_0}$. As depicted in Figure S3b, a significant portion of the radiation from the electric dipole emitter is coupled to the AgNW waveguide, attributable to the high density of state in the SPP.

4. Simulations for plasmonic trapping force

In this simulation, a 100-nm-radius AgNW is placed in water as the surrounding medium. A HE_1 SPP mode, with the power set at 1mW, is excited at the port of the AgNW, to mimic the SPP coupled from the linearly polarized photonic mode (LP_{01}) in the tapered optical fiber in the experiment. It is worth noting that, as shown in Figure S4a, the TM_0 SPP mode (orange line) on the AgNW waveguide in water has an effective mode index (n_{eff}) larger than that of the optical fiber (n_{glass}, blue curve). Therefore, the LP_{01} mode in a tapered optical fiber can not efficiently excite the TM_0 SPP mode through Landau-Zener tunneling, but only excite the HE_1 SPP mode (red line) through mode index matching. The plasmonic trapping force is calculated by integrating the Maxwell stress tensor[4] on all surfaces of the virtual box (with a length of 42 nm) with dielectric index n = 2.42 to mimic diamond. Maxwell stress tensor is defined as:

$$\overleftrightarrow{\boldsymbol{T}} = \begin{bmatrix} \varepsilon E_x^2 + \mu H_x^2 - \dfrac{\varepsilon E^2 + \mu H^2}{2} & \varepsilon E_x E_y + \mu H_x H_y & \varepsilon E_x E_z + \mu H_x H_z \\ \varepsilon E_y E_x + \mu H_y H_x & \varepsilon E_y^2 + \mu H_y^2 - \dfrac{\varepsilon E^2 + \mu H^2}{2} & \varepsilon E_y E_z + \mu H_y H_z \\ \varepsilon E_z E_x + \mu H_z H_x & \varepsilon E_z E_y + \mu H_z H_y & \varepsilon E_z^2 + \mu H_z^2 - \dfrac{\varepsilon E^2 + \mu H^2}{2} \end{bmatrix}$$

The optical force can then be calculated through

$$\vec{\boldsymbol{F}}_{total} = \iint \overleftrightarrow{\boldsymbol{T}} \cdot \hat{\boldsymbol{n}} d\boldsymbol{A}$$

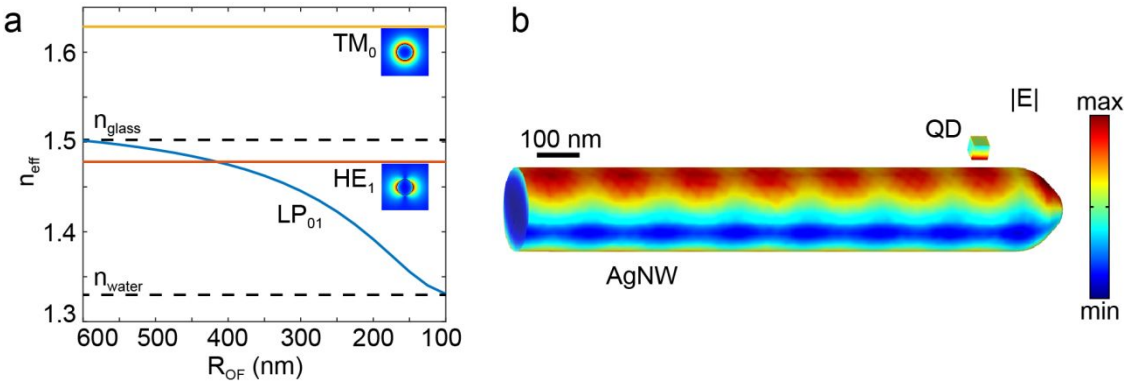

Figure S4. Trapping potential analysis. (a) The $HE_{\pm1}$ mode (red) is chosen for plasmonic trapping, since it is the only mode with the effective index covered by that of the tapered optical fiber (blue). The effective mode index of TM_0 mode (orange) is always higher than the mode index of the optical fiber, and thus cannot be excited. The AgNW radius is set at 100 nm in this simulation. (b) The electric field distribution on the AgNW surface. The periodic pattern is due to the interference between the incident SPP and the tip-reflected SPP.

5. Optical setup for fluorescent decay curve measurements

The time-resolved fluorescence measurement is conducted by the time-correlated single photon counting method. As shown in Figure S5, a 1030 nm laser with 76 MHz repetition rate and ~90 fs pulse duration, is generated by an oscillator (Light Conversion Inc., Pharos) and frequency-doubled to 515 nm in wavelength. The laser pulses were coupled into the optical fiber of the OF-AgNW probe to excite the PL from the FND assembled to the AgNW tip. The fluorescence signals are collected through free space by an objective lens (40×, 0.6 NA) and detected by an avalanche photodiode (PicoQuant, PDM) and its temporal trace is measured by a time-correlated single photon counting module (PicoQuant, PicoHarp 300).

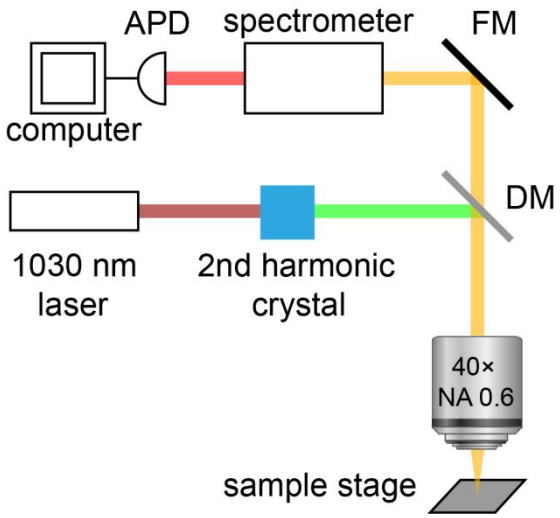

Figure S5. The schematic of the Optical setup for time-resolved fluorescence measurement. APD: avalanche photodiode, FM: flip mirror, DM: dichroic mirror.

6. Estimation of fluorescent intensity enhancement

After trapped on an AgNW, the FND exhibits a PL intensity averaging approximately 582 ± 50 kcps, as shown in Figure S6b. The FND PL without plasmonic enhancement were conducted with FNDs attached to bare tapered optical fibers. This was achieved by immersing the fibers into high concentration FND solutions and subsequent drying in air. By increasing the excitation power a hundredfold, from 1mW to ~100mW, the experiments yielded an average PL intensity of about 26

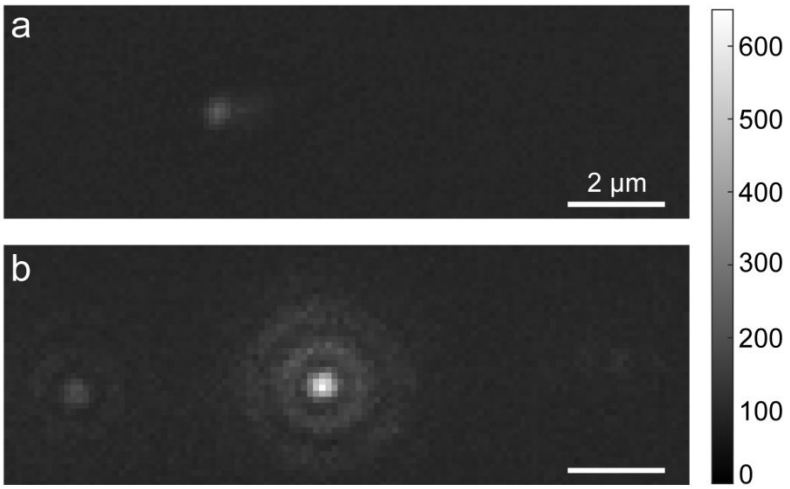

Figure S6. Optical images of NV centers trapped (a) on a bare optical fiber (integration time: 100 ms), and (b) on AgNW (integration time: 35 ms).

kcps. From these observations, the intensity enhancement factor is deduced to be around 2200.

References

1. Chen, Y.; Nielsen, T. R.; Gregersen, N.; Lodahl, P.; Mørk, J., Finite-element modeling of spontaneous emission of a quantum emitter at nanoscale proximity to plasmonic waveguides. *Physical Review B* **2010,** *81* (12), 125431.
2. Collins, S. S. E.; Searles, E. K.; Tauzin, L. J.; Lou, M.; Bursi, L.; Liu, Y.; Song, J.; Flatebo, C.; Baiyasi, R.; Cai, Y.-Y.; Foerster, B.; Lian, T.; Nordlander, P.; Link, S.; Landes, C. F., Plasmon Energy Transfer in Hybrid Nanoantennas. *ACS Nano* **2021,** *15* (6), 9522-9530.
3. Kimmitt, N.; Wertz, E. A., Tracking the Coupling of Single Emitters to Plasmonic Nanoantennas with Single-Molecule Super-Resolution Imaging. *ACS Photonics* **2021,** *8* (4), 1020-1026.
4. Jackson, J. D., *Classical electrodynamics*. New York, Wiley: 1999.